

# Measurement of high quality factor superconducting cavities in tesla-scale magnetic fields for dark matter searches

S. Posen<sup>1a</sup>, M. Checchin<sup>1</sup>, O.S. Melnychuk<sup>1</sup>, T. Ring<sup>1</sup>, I. Gonin<sup>1</sup>

<sup>1</sup>*Fermi National Accelerator Laboratory, Batavia, Illinois, 60510, USA*

In dark matter searches using axion haloscopes, the search sensitivity depends on the quality factors ( $Q_0$ ) of radiofrequency cavities immersed in multi-tesla magnetic fields. Increasing  $Q_0$  would increase the scan rate through the parameter space of interest. Researchers developing superconducting radiofrequency cavities for particle accelerators have developed methods for obtaining extremely high  $Q_0 \sim 10^{11}$  in  $\mu\text{T}$ -scale magnetic fields. In this paper, we describe efforts to develop high  $Q_0$  cavities made from conventional superconductors, starting from a particle accelerator-style cavity and then exploring a more optimized geometry for the application. A quality factor of  $(5.3 \pm 0.3) \times 10^5$  is obtained at 3.9 GHz and 6 T at 4.2 K.

## I. INTRODUCTION

Superconducting radiofrequency (SRF) cavities have been used in particle accelerator applications for decades, and substantial research efforts have gone into developing techniques to maximize cavity performance, in particular the quality factor  $Q_0$ —which determines the heat dissipated to the cryogenic systems—and the accelerating gradient  $E_{\text{acc}}$ —which determines the energy gain per unit length [1]. Modern SRF cavities can routinely achieve  $Q_0$  on the order of  $10^{11}$  and  $E_{\text{acc}}$  on the order of 40 MV/m.

Axion haloscopes use radiofrequency cavities to search for dark matter [2]. Cavities are placed in magnetic fields on the order of several tesla. Theoretical models for axions [3]–[5] predict that, if they exist as dark matter [6]–[8], there is a chance that passing axion particles will be converted to photons, with frequency related to the axion mass (for a review see [9]). If the frequency of the cavity matches that of photons converted from axions, a small signal may be detectable. By tuning the cavity frequency, different potential axion masses can be evaluated. The signal predicted is extremely small, and there is a large mass range of interest. As a result, researchers are developing ways to achieve high sensitivity within a short sampling time for a given frequency, so that the scan rate can be as high as possible, allowing wide ranges to be scanned within reasonable experimental timeframes. The scan rate is proportional to  $B_a^4 V^2 C^2 Q_{\text{eff}} T^{-2}$ , where  $B_a$  is the applied magnetic field strength inside the cavity,  $V$  is the cavity volume,  $C$  is a geometric form factor related to the RF electric field distribution and its alignment with the applied

magnetic field (the axion couples to  $\mathbf{E}_{\text{RF}} \cdot \mathbf{B}_a$ , where  $\mathbf{E}_{\text{RF}}$  is the RF electric field),  $Q_{\text{eff}}$  is the effective quality factor of the cavity, and  $T$  is the system noise temperature.  $Q_{\text{eff}}$  is a factor that depends on  $Q_0$ ,  $Q_{\text{ext}}$ , and  $Q_a$ , where  $Q_{\text{ext}}$  is the external quality factor (which depends on the coupling to the cavity) and  $Q_a$  is the effective quality factor of the galactic axion field  $\sim 10^6$ . There is a benefit to  $Q_{\text{eff}}$  to increasing  $Q_0$  up to a value close to  $Q_a$  and also beyond [10].

The dependence on quality factor makes the use of SRF cavities a possible avenue for increasing scan rate. Past experiments have typically used copper cavities, including ADMX and HAYSTAC [11], [12], with typical  $Q_0$  values  $\sim 10^4$ – $10^5$  depending on the frequency. Early efforts on SRF cavities have been showing promising results, in particular by coating copper or aluminum cavities with superconductors like  $\text{Nb}_3\text{Sn}$ ,  $\text{NbTi}$ , and  $\text{YBCO}$  [13]–[15]. Promising results have also been obtained by using dielectrics to screen fields from the walls of copper cavities [16], [17]. In this paper, we present high magnetic field  $Q_0$  measurements of SRF cavities that were fabricated with methods that are different than those studied previously. The first method uses a vapor diffusion technique to coat niobium cavities with an inner layer of  $\text{Nb}_3\text{Sn}$ . This method is used to coat cavities for particle accelerators that can operate with high  $Q_0$  at higher temperatures than cavities made from the standard material Nb [18]. The second technique is to machine a cavity shape out of solid  $\text{NbTi}$ . High magnetic field measurements are presented below, after discussing dissipation mechanisms, cavity designs, and the experimental apparatus.

<sup>a</sup>Email: sposen@fnal.gov

## II. MAGNETIC FLUX DISSIPATION IN RF SUPERCONDUCTORS

SRF cavities provide orders of magnitude higher  $Q_0$  than copper in accelerator applications, but the operating conditions for haloscopes are substantially different. SRF cavities in accelerators are typically made of niobium and operate at  $\sim 2$  or  $\sim 4$  K, and in magnetic field environments  $\sim 1$   $\mu$ T. Under these conditions, the niobium walls are primarily in the Meissner state, with some small amount of trapped flux from the ambient field during cooldown. As a result, the surface resistance  $R_s$ , which determines  $Q_0$  by  $Q_0 = G/R_s$ , where  $G$  is a geometry-dependent factor that is independent of frequency, generally is dominated by the temperature-dependent BCS resistance [19] and by trapped flux surface resistance: under the influence of RF currents, flux trapped in the superconductor during cooldown undergoes motion, which generates dissipation [20], [21].

In haloscopes, cavities are operated at tens or hundreds of mK to reduce the noise temperature, where the BCS resistance is exponentially suppressed. However, the magnetic field is typically several tesla, above the upper critical field of niobium, which would leave it in the normal conducting state. Superconductors with substantially higher critical fields are required to maintain superconductivity, such as those used in superconducting magnets, like Nb<sub>3</sub>Sn, NbTi, YBCO, and MgB<sub>2</sub>. Under these conditions, these superconductors would not be in the Meissner state but in the vortex state, with substantial amounts of flux in the superconductor. This is expected to be the dominant source of surface resistance. The Lorentz force per unit length  $f_L$  experienced by a vortex in the superconducting wall with local RF surface current density  $\mathbf{J}$  is  $f_L = \mathbf{J} \times \Phi_0$ , where  $\Phi_0$  is the flux quantum and the vector  $\Phi_0$  is aligned with the normal vector to the cavity surface ( $\hat{\mathbf{n}}$ ). The total flux per unit of area ( $\Phi = N\phi_0$ ) is proportional to the projection of the applied magnetic field  $\mathbf{B}_a$  along the surface normal vector ( $\mathbf{B}_a \cdot \hat{\mathbf{n}}$ ) and defines the local areal density of vortices ( $N$ ). The more the cavity surface is parallel to  $\mathbf{B}_a$ , the lower is the local vortex areal density and the lower is the local power dissipation.

## III. CAVITY GEOMETRIES

The first cavity geometry chosen to study was that of TESLA [22], shown in Figure 1. This geometry is widely used in particle accelerators, including for

example the European XFEL and LCLS-II [23], [24]. This geometry is optimized for accelerators, not for high magnetic fields, but existing cavities were on hand to conduct first experiments. In Appendix 1, it is shown that on a cavity of this shape, substantial flux losses occur in regions where the cavity surface is nearly perpendicular to the applied field. The accelerating mode would also be the mode relevant for axion searches, the fundamental TM010 mode of the cavity.

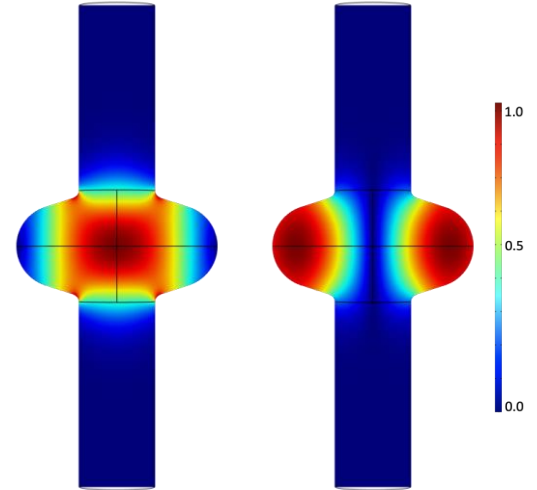


Figure 1: Normalized electric (left) and magnetic (right) field intensity of the TM010 mode in a cross section through the middle of a TESLA cavity used in particle accelerators [22].

While first studies were being set up on the TESLA cavity, a new cavity geometry was developed and began fabrication. The design process involved experimenting with different shapes to try to minimize the fraction of current that was oriented perpendicular to the applied field ( $J_\perp$ ), while still maintaining an RF electric field that is highly parallel to the applied DC magnetic field. A cigar shaped cavity was chosen out of the different geometries evaluated, and Appendix 2 shows part of the optimization process to minimize the perpendicular component of the current. The cigar-shaped geometry is shown in Figure 2. The relevant mode for axion searches is the TM010 mode, which is the ninth-lowest frequency mode of the cavity, above four degenerate TE11n modes. The geometric form factor  $C$  for the TM010 mode is simulated to be 0.499 and the RF volume is  $5.05 \times 10^{-4}$  m<sup>3</sup>.

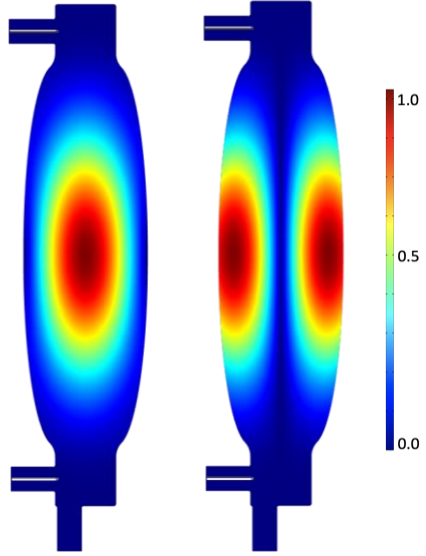


Figure 2: Normalized electric (left) and magnetic (right) field intensity of the TM010 mode in a cross section through the middle of the cigar geometry cavity developed as part of this work.

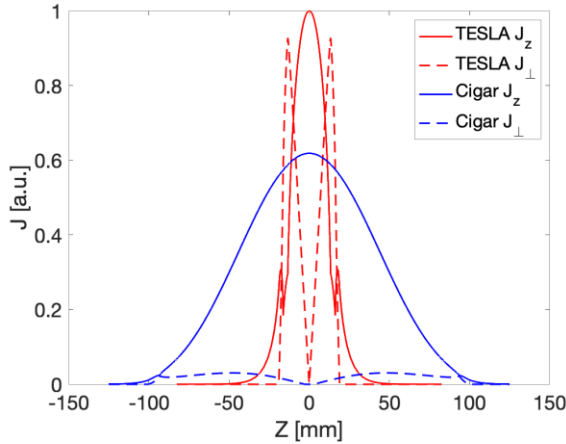


Figure 3: Comparison of parallel ( $J_z$ ) and perpendicular ( $J_{\perp}$ ) currents (relative to the applied DC magnetic field) in the TESLA and cigar-shaped cavities. The cigar-shaped cavity was designed to have  $J_z$  significantly smaller than  $J_{\perp}$ .

#### IV. EXPERIMENTAL APPARATUS

The high magnetic field test stand available for carrying out the measurements was an Oxford Teslatron™ system at Fermilab [25], which previously has mainly been used to test wires for superconducting magnet application. It has a NbTi solenoid magnet capable of reaching  $\sim 6$  T with a 147 mm bore and is operated in liquid helium. A special insert was fabricated that allowed for a cavity to be assembled and evacuated in a cleanroom, then inserted into the dewar. The system is shown in Figure 4.



Figure 4: Teslatron™ system at Fermilab including cryostat (background) and solenoid (foreground). The inset shows the cavity insert with the 3.9 GHz Nb<sub>3</sub>Sn TESLA cavity installed.

In this system, the solenoid current is measured, and converted to peak applied magnetic field on the central axis based on information from the vendor. Cavities are assembled with two antennae attached to feedthroughs. Coaxial cables bring the signal through the helium volume to feedthroughs on the top plate, which in turn are connected to a vector network analyzer. The network analyzer is used to measure the loaded quality factor  $Q_L$  by fitting the resonance curve in transmission through the cavity. The signal map is shown in Figure 5.

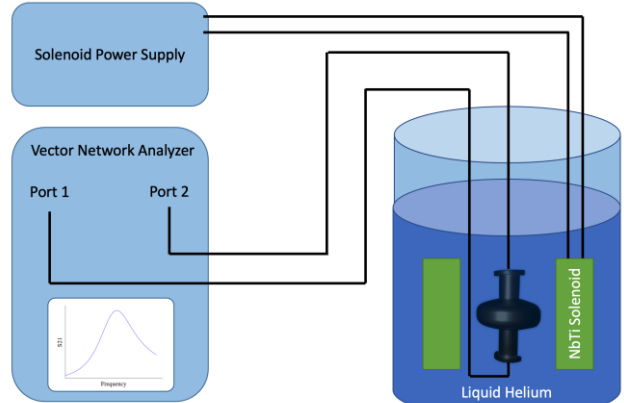


Figure 5: Signal map for high magnetic field  $Q_L$  measurement.

Figure 6 shows a magnetic field intensity map of the solenoid (map was simulated based on coil position and should be considered approximate) as well as how the cavities are designed to be positioned inside of the system. The solenoid is closed on the bottom, and the TESLA cavity position had to be raised slightly higher than the region of maximum field intensity to fit above the bottom plate with the RF hardware attached. The figure illustrates how the

magnetic field lines cross the TESLA cavity nearly perpendicularly to the surface, while they are nearly parallel to the surface of the cigar-shaped cavity, particularly where the RF currents and the DC field are highest.

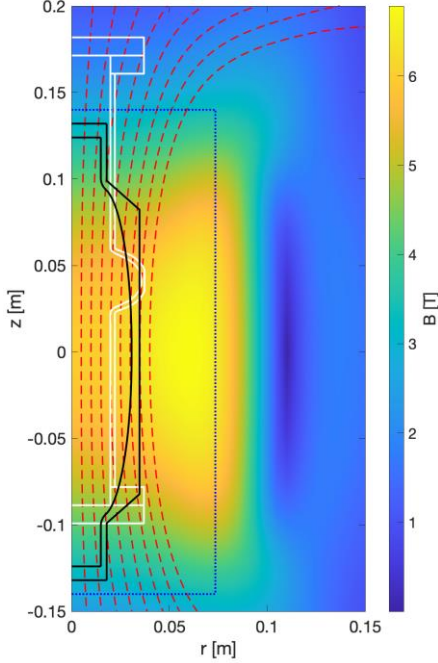


Figure 6: Calculated magnetic field intensity inside the dewar when the center of the solenoid is at 6 T.  $R=0$  corresponds to the axis of symmetry. The dotted blue line shows the boundary of the region inside the solenoid. The red dashed lines are a selection of magnetic field lines. The white solid line is the outline of the TESLA cavity positioned as expected in the system, and the black outline similarly is for the cigar-shaped cavity.

The Fermilab particle accelerator research program had already generated Nb<sub>3</sub>Sn TESLA cavities with frequency 1.3 GHz and 3.9 GHz. The 3.9 GHz cavity was chosen because it fit in the bore of the solenoid ( $\sim 4$  GHz is also an interesting frequency for future axion studies, e.g., [26]). For direct comparison, 3.9 GHz was also chosen for the frequency at which to fabricate the cigar-shaped cavities.

The previous performance of the 3.9 GHz TESLA cavity is shown in Figure 7. The performance was measured at 4.4 K after cooldown in a  $< 1 \mu\text{T}$  magnetic field. The Nb<sub>3</sub>Sn cavity started as a niobium cavity, which was electropolished, then Nb<sub>3</sub>Sn vapor diffusion coated, as described in [18], then rinsed with high pressure ultrapure water, and assembled in a class 10 cleanroom prior to measurement.

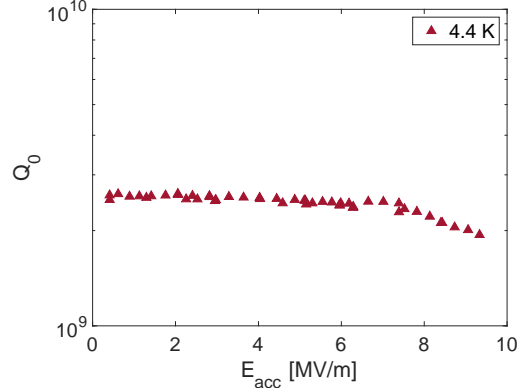


Figure 7: Previous performance of Nb<sub>3</sub>Sn TESLA cavity, after cooldown in a  $< 1 \mu\text{T}$  magnetic field

To prepare for the high magnetic field measurement, the TESLA cavity was disassembled from its previous assembly, high pressure rinsed, then assembled in a cleanroom to the insert shown in Figure 4.



Figure 8: Side view of the electropolishing setup for the cigar-shaped cavity. The aluminum anode is lowered from above; it was fabricated with geometry to match the cavity.

The Nb<sub>3</sub>Sn cigar-shaped cavity was milled from a pair of solid blocks of reactor-grade niobium. NbTi flanges were then welded to its ports. The cavity was then electropolished using a typical niobium SRF cavity electropolishing process [27], with a specially shaped aluminum anode and corresponding fixturing, shown in Figure 8. The cavity was coated with Nb<sub>3</sub>Sn, then rinsed with high pressure ultrapure water, and assembled for measurement.



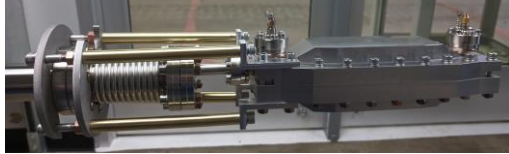


Figure 9: Top: Cigar-shaped cavity after Nb<sub>3</sub>Sn coating. Bottom: Cigar-shaped Nb<sub>3</sub>Sn cavity assembled to the test insert.

The NbTi cigar-shaped cavity was milled from a pair of solid blocks of NbTi. The material used was high-homogeneity NbTi from ATI metals [28]. The material is produced with precautions to avoid micro-inhomogeneities, such as Nb inclusions. It is then checked using radiography standards developed for the production of high homogeneity NbTi wire for accelerator magnet applications [29]. After milling the blocks, NbTi flanges were welded to it. This cavity was not electropolished due to concerns of the removal process affecting Nb and Ti differently. Instead, the cavity was just degreased, high pressure water rinsed, and assembled to the test insert.

## V. RESULTS

The main results of this work are shown in Figure 10. Results are given in terms of  $Q_L$  vs applied magnetic field  $B_a$ . The applied magnetic field is the peak DC field that would be expected to be measured on the central axis of the solenoid. All cavities were cooled down with near-zero current in the solenoid, then the current was increased in steps. The  $Q_L$  was measured by the network analyzer. At low  $B_a$ ,  $Q_L$  is expected to be determined by a combination of the external quality factors  $Q_{ext}$  of the coupling ports ( $Q_L^{-1} = Q_0^{-1} + Q_{ext1}^{-1} + Q_{ext2}^{-1}$ ) and the intrinsic quality factor  $Q_0$ , which is expected to be strongly influenced by trapped flux surface resistance from during the cooldown of the cavity (from Earth's magnetic field and from residual magnetization in the dewar). At high  $B$ ,  $Q_L$  is expected to be dominated by  $Q_0$  of the cavity.  $Q_{ext}$  values were chosen to be at least an order of magnitude above the expected range of  $Q_0$  so that it wouldn't contribute significantly to the overall  $Q_L$  at high fields, but still low enough that the power coupled between the antennae and the cavity would provide a strong signal. For the TESLA cavity the  $Q_{ext}$  values were measured to be  $(3.4 \pm 0.5) \times 10^8$  and  $(2.3 \pm 0.3) \times 10^8$ . For the cigar-shaped cavities the  $Q_{ext}$  values were measured to be  $(8.2 \pm 4.1) \times 10^8$  and  $(7.4 \pm 3.7) \times 10^8$  (there was higher uncertainty in measuring  $Q_{ext}$  values at room temperature for the cigar cavity due to other modes close to the TM010 mode).

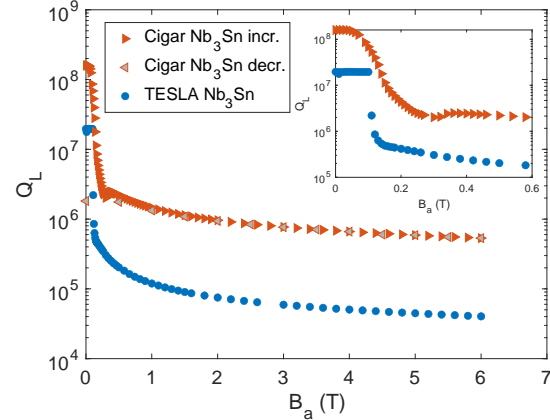


Figure 10: Loaded quality factor vs applied magnetic field data for the TESLA and cigar-shaped Nb<sub>3</sub>Sn cavities. The inset provides a zoom of the low field region. For the cigar-shaped Nb<sub>3</sub>Sn cavity, measurements were made both for increasing and for decreasing field.

For the Nb<sub>3</sub>Sn-coated Nb cavities, the niobium bulk influenced the behavior at low fields. The niobium acted as a Meissner shield to the applied field until around 0.1 T, at which point it appears that flux begins to penetrate the niobium walls. This is approximately half of the nominal field at which flux penetration is expected for niobium, with the difference likely due to demagnetization effects. After flux penetrates, the  $Q_0$  decreases steadily with increasing field, then begins to start decreasing more slowly towards higher applied fields, particularly above  $\sim 3$  T. By the time the cavities reach 6 T, the TESLA cavity  $Q_0$  is  $(4.3 \pm 0.2) \times 10^4$ , and the cigar-shaped Nb<sub>3</sub>Sn cavity  $Q_0$  is  $(5.3 \pm 0.3) \times 10^5$  (this assumes that  $Q_L \approx Q_0$  in this range).

At the maximum applied field of 6 T, the incident power from the network analyzer was lowered to evaluate if it would alter the measurement. The power was adjusted from 10 dBm to 0 dBm and then to -10 dBm. For each cavity, no change in  $Q_0$  was observed within uncertainty for these 3 power levels.

For the cigar shaped Nb<sub>3</sub>Sn cavity, after reaching the peak field of 6 T, the field was decreased in steps to check for hysteresis. The increasing curve was followed until the field was decreased to  $\sim 0.5$  T. At low field values, the  $Q_L$  was smaller than for the increasing curve, suggesting additional trapped flux was present compared to after cooldown.

The frequency change vs applied magnetic field data is shown in Figure 11. The cavities were not tuned exactly to 3.9 GHz – the zero-field frequency  $f_0$  for the TESLA Nb<sub>3</sub>Sn cavity was 3870 MHz.  $f_0$  for the cigar-

shaped Nb<sub>3</sub>Sn cavity was 3891 MHz. The frequency of the cigar-shaped cavity changed less at higher fields. This may be due to the stiffer cavity resulting in smaller cavity deformation from magnetic forces.

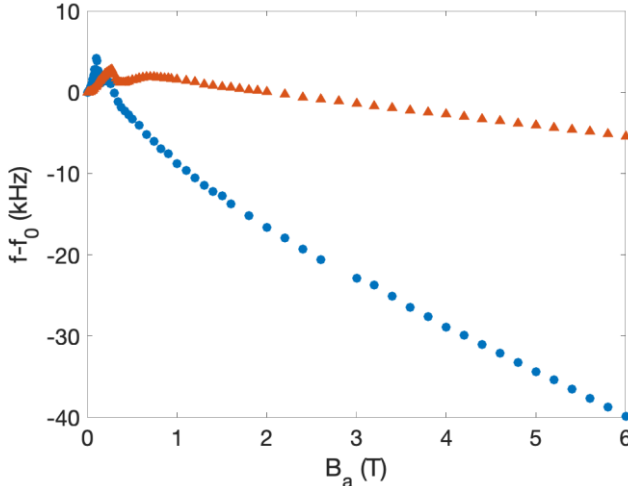


Figure 11: Frequency vs applied magnetic field data for the TESLA and cigar-shaped Nb<sub>3</sub>Sn cavities.

## VI. DISCUSSION

The highest  $Q_0$  reported in this study at 6 T is  $(5.3 \pm 0.3) \times 10^5$  for the Nb<sub>3</sub>Sn cigar shaped cavity. The surface resistance for a high purity copper cavity at the same temperature, magnetic field, and frequency can be calculated based on theoretical models using the tool from Ref. [30] to be  $0.0029 \Omega$  (this may be an optimistic value – practical factors may result in a somewhat higher surface resistance). Using this surface resistance and the same geometry factor as the cigar cavity would yield a  $Q_0$  of  $1.6 \times 10^5$ , a factor of 3.4 lower than the Nb<sub>3</sub>Sn cigar shaped cavity. This suggests that the use of Nb<sub>3</sub>Sn coatings could be a promising direction for improving axion search scan rate near this frequency. It may also improve at lower temperatures.

The results presented here are compared to several previous studies of superconducting cavities in high magnetic fields in Table 1. It should be noted in these comparisons that differences in frequency, cavity geometry, and magnetic field value could substantially impact the  $Q_0$  value. The previous materials studied included conventional superconductors like NbTi as well as high temperature superconductors like REBCO (RE stands for a rare earth metal such as Y). The  $Q_0$  values reported from this study are the highest of those in the table, but also the frequency is substantially lower than the other cavities, which likely contributes to smaller flux losses. Overall, superconducting cavities appear to be a promising

avenue to increasing  $Q_0$  in high magnetic fields, including the Nb<sub>3</sub>Sn coatings developed for accelerator applications. The difference in performance between the TESLA and cigar-shaped cavities show the importance of selecting an appropriate geometry that takes into account flux losses in the superconducting material.

Table 1: Comparison of the results from this work to several previous studies of superconducting cavities in high magnetic fields for axion research.

Source	Material	$f$ (GHz)	$B_a$ (T)	$T$ (K)	$Q_0$
This work	Nb <sub>3</sub> Sn	3.9	6.0	4.2	$(5.3 \pm 0.3) \times 10^5$
[13]	NbTi/Cu	9.08	5	4.2	$2.95 \times 10^5$
[14]	Nb <sub>3</sub> Sn	9	8	4.2	$6 \times 10^5$
[14]	REBCO	9	11.6	4.2	$7 \times 10^4$
[15]	YBCO	6.93	8.0	4.2	$1.5 \times 10^5$

Another recent result of a novel cavity developed to achieve high  $Q_0$  in high magnetic fields is the 10.3 GHz dielectric resonator from di Vora et al. [16], which has a  $Q_0$  of  $9 \times 10^6$  at 4.2 K in a 8 T magnetic field. They use cylindrical dielectrics to screen the field from the copper walls, meaning that there is a significant volume of the cavity with low RF field amplitude and therefore weak axion sensitivity. However, the high  $Q_0$  can have a stronger overall impact to sensitivity, particularly at high frequencies  $\sim 10$  GHz and above.

Axion search scan rate scales with the fourth power of magnetic field, and fields significantly higher than 6 T are readily achievable, though not in the measurement system used in this paper. The  $Q_0$  of the Nb<sub>3</sub>Sn cigar shaped cavity was decreasing relatively slowly with field at 6 T, and it may remain quite high up to higher magnetic fields. For example, between 4 T and 6 T, the  $Q_0$  decreased from  $6.6 \times 10^5$  to  $5.3 \times 10^5$ . If this continued linearly, it would result in a  $Q_0$  of  $4.3 \times 10^5$  at 8 T. The upper critical field of Nb<sub>3</sub>Sn is substantially higher,  $\sim 30$  T for near-optimal stoichiometry [31].

There are some simple next steps for this experimental program. The first will be to test the cigar shaped NbTi cavity and compare its performance to the Nb<sub>3</sub>Sn cavities. The second will be to install a pump in the cryogenic system, which will allow future measurements to be performed also below 4 K, where pinning strength may be improved, and possibly also  $Q_0$ . The third will be to evaluate the impact of small misalignments and inhomogeneities of the applied field.

For longer-term next steps, work is underway to develop a tunable superconducting cavity geometry with surface currents highly parallel to the applied field, as they are in the cigar shape. In addition, studies

will be performed to modify the Nb<sub>3</sub>Sn coating process to try to increase pinning strength. Finally, procurement is underway for a millikelvin high magnetic field test stand, where studies can be performed under temperature and magnetic field conditions as close as possible to a dark matter search.

The results presented here will also be compared to existing theoretical models for SRF cavities in magnetic fields. This may help to improve the models including in regimes relevant for particle accelerators.

## VII. SUMMARY

Nb<sub>3</sub>Sn SRF cavity technology developed for particle accelerators was studied at multi-tesla DC magnetic fields for dark matter search applications. A cigar-shaped geometry was developed to have currents that flow mostly parallel with the applied magnetic field to reduce flux dissipation. A Nb<sub>3</sub>Sn coated cavity with the cigar-shaped geometry had a  $Q_0$  of  $(5.3 \pm 0.3) \times 10^5$  at 6 T and 4.2 K. A Nb<sub>3</sub>Sn coated cavity with a geometry typical of accelerator applications had a  $Q_0$  of  $(4.3 \pm 0.2) \times 10^4$  at 6 T and 4.2 K. A higher  $Q_0$  in this regime can help to improve scan rates for axion haloscopes.

## VIII. ACKNOWLEDGEMENTS

The authors would like to thank the many people who contributed to the results presented in this paper. Thanks to Vadim Kashikin for extremely useful discussions of flux behavior in superconducting materials under multi-tesla fields, including important safety aspects of this experiment. Thanks to Vito Lombardo for sharing a model of the field inside the solenoid. Thanks to Eddie Pieszchala, Mike Foley, and the Fermilab machine shop for cavity fabrication. Thanks to Daniele Turrioni, Al Rusy, and Sean Johnson, who run the lab with the 6 T magnet, and carried out the installation of the cavity insert to the solenoid and operation of the magnet and cryo system. Thanks to the ADMX collaboration, especially Andrew Sonnenschien and Daniel Bowring, who partially supported the fabrication of the cavity insert and who contributed to the investigations of the effects of putting large masses of superconducting material in the magnet. Thanks to Scott Adams and Tedd Ill for assembly of the cavities to the insert. Thanks to Brad Tennis for carrying out coating of the Nb<sub>3</sub>Sn cavities and initial setup of the cavity insert. Thanks to Anna Grassellino, Alex Romanenko, Raphael Cervantes, and Roni Harnik of Fermilab, Jim Sauls, Venkat Chandrasekhar, and Bill Halperin of Northwestern

University and Phil O'Larey and Miles Naughton of ATI Metals for useful discussions. This work was supported by the United States Department of Energy, Office of High Energy Physics under Contracts DE-AC05-06OR23177 Fermilab. This material is based upon work supported by the U.S. Department of Energy, Office of Science, National Quantum Information Science Research Centers, Superconducting Quantum Materials and Systems Center (SQMS) under contract number DE-AC02-07CH11359.

## APPENDIX A: MEASUREMENTS WITH 100 $\mu$ T APPLIED FIELD

As an initial evaluation of  $Q_0$  of an SRF cavity in a magnetic field, a 1.3 GHz Nb<sub>3</sub>Sn coated TESLA cavity was tested after cooldown with an applied magnetic field of 100  $\mu$ T, generated by Helmholtz coils around the cavity (Helmholtz coils can be seen in Figure A1). The cavity was cooled slowly and uniformly to try to fully trap the applied field and avoid thermocurrents [32], [33]. Other instrumentation around the cavity included a temperature map (or T-map), an array of 540 thermometers placed over the surface of the cavity (see [34] for more information about T-mapping of SRF cavities). Figure A2 shows an azimuthal cross section of the cavity with the approximate location of the temperature sensors along its surface. The cavity and RF fields are axisymmetric about R=0. There are 36 boards, each with 15 sensors, located 10 degrees apart azimuthally. The RF magnetic field strength is approximately the same (within ~5%) for the middle 11 sensors, and somewhat lower for the two each at the top and bottom of the cavity (~83% and ~62% of the peak surface magnetic field value).



Figure A1: A 1.3 GHz cavity with Helmholtz coils around it.

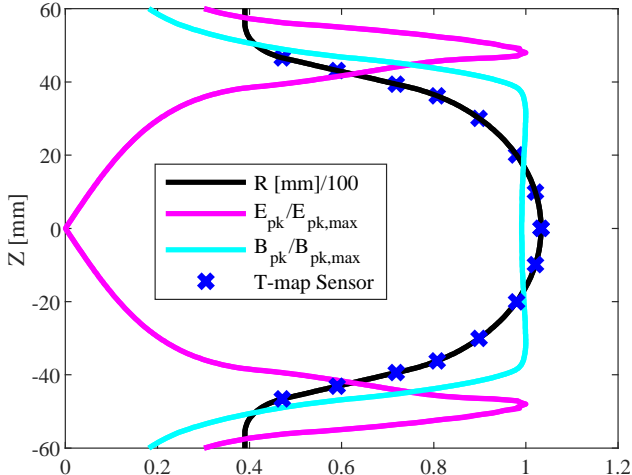


Figure A2: Temperature map sensor locations around an azimuthal slice of the cavity. There are 36 such slices around the cavity.

A temperature map measured at an accelerating gradient of 9.9 MV/m and a temperature of 1.6 K is shown in Figure A3. The  $\Delta T$  values are given relative to the ambient bath temperature. The quality factor was measured to be  $2.1 \times 10^8$ , substantially lower than typical values between  $10^{10}$  and  $10^{11}$  at this temperature, indicating high surface resistance due to trapped flux. The T-map shows where the surface resistance was high and where it was low: surface temperature rise is proportional to the local RF power dissipation. There is high heating in regions where the applied magnetic field is more perpendicular to the RF surface currents and lower where they are more parallel. This indicates that the TESLA geometry is expected to have substantial  $Q_0$  degradation from the perpendicular regions when cooled in a large magnetic field. The sensors very close to the top and bottom of the cavity have low values because of the lower RF magnetic field in those regions of the surface (see Figure A2).

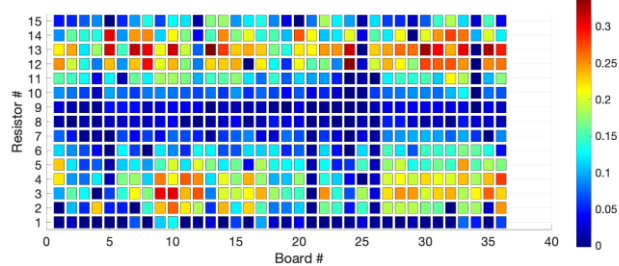


Figure A3: Temperature map of the 1.3 GHz Nb<sub>3</sub>Sn cavity cooled in a 100  $\mu$ T field, with 9.9 MV/m accelerating gradient at 1.6 K and a  $Q_0$  of  $2.1 \times 10^8$ .

In addition to T-map data,  $Q_0$  vs  $E_{acc}$  data were measured. Measurements were made at high fields using typical SRF power balance methods [35] as well as with low power decays [36]. An example of a decay measurement is plotted in Figure A4, in which the slope of the transmitted power vs time is used to determine  $Q_L$ . Then the  $Q_{ext}$  values determined from the power balance measurements are used to convert from  $Q_L$  to  $Q_0$ . The  $Q_0$  vs  $E_{acc}$  data are plotted in Figure A5.

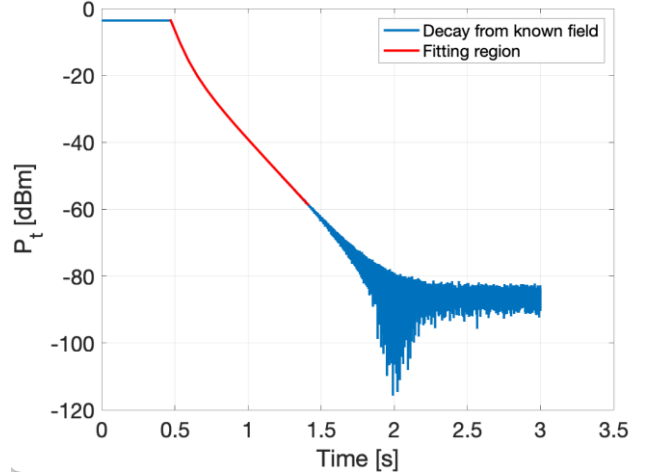


Figure A4: Example of a low power decay from a known field. The red line shows where the data was fit to extract  $Q_0$  values vs field at low  $E_{acc}$ .

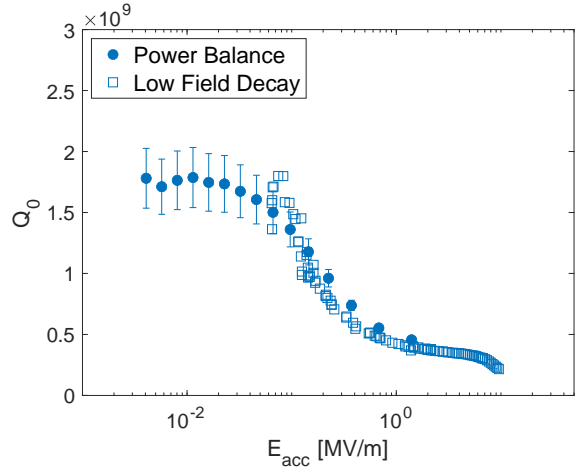


Figure A5:  $Q_0$  vs  $E_{acc}$  data measured using two methods: power balance and low field decays. The observed change in  $Q_0$  may be related to depinning of trapped flux at fields above  $E_{acc} \sim 0.1$  MV/m.

There is a transition that occurs between  $\sim 0.01$  MV/m and  $\sim 1$  MV/m, in which the  $Q_0$  decreases from  $\sim 2 \times 10^9$  to  $\sim 3 \times 10^8$ . This may be related to dissipative depinning of flux in the Nb<sub>3</sub>Sn (see for example measurements in [37]) at higher RF fields. The fields

used here (even down to 0.01 MV/m) are significantly higher than would be needed for axion applications, and higher than are excited by the network analyzer in the high magnetic field measurements of the 3.9 GHz cavities.

## APPENDIX B: CIGAR GEOMETRY DEVELOPMENT

To develop a geometry that would have high  $Q_0$  in magnetic fields, the chosen starting point was a cylinder operating in the TM010 mode at 3.9 GHz with length maximized to the available space in the solenoid. Different types of ends were examined for the cylinder, including conical ends and elliptical ends. The optimization process for the elliptical-ended cavity is shown in Figure B1, showing that a ratio  $a/b$  of  $\sim 3$  would be optimal to minimize the perpendicular component of the surface current (optimization done in Comsol [38]). For each of the different models under consideration, the stored energy in the cavity was always normalized to 1 J. Later additions included narrow cylindrical sections on the ends of the cavity to further reduce the perpendicular current and provide a low-field space for adding antennas.

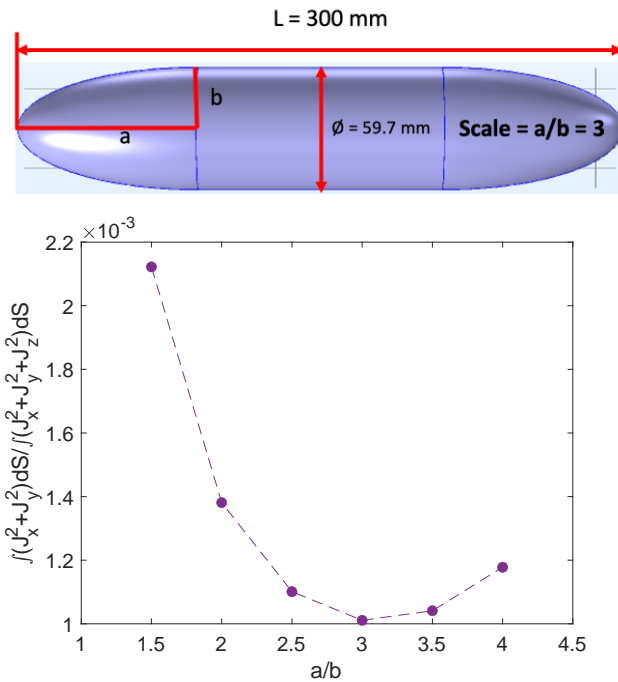


Figure B1: Optimization process for the elliptical-ended cylinder that became the cigar-shaped cavity. The minimization target was the ratio of the surface integral of the perpendicular current density to the surface integral of the total current density.

## IX. REFERENCES

- [1] H. Padamsee, “50 years of success for SRF accelerators - A review,” *Supercond. Sci. Technol.*, vol. 30, no. 5, (2017).
- [2] P. Sikivie, “Experimental tests of the ‘invisible’ axion,” *Phys. Rev. Lett.*, vol. 51, no. 16, 1415–1417, (1983).
- [3] R. D. Peccei and H. R. Quinn, “CP conservation in the presence of pseudoparticles,” *Phys. Rev. Lett.*, vol. 38, no. 25, 1440–1443, (1977).
- [4] R. D. Peccei and H. R. Quinn, “Constraints imposed by CP conservation in the presence of pseudoparticles,” *Phys. Rev. D*, vol. 16, no. 6, 1791–1797, (1977).
- [5] S. Weinberg, “A New Light Boson?,” *Phys. Rev. Lett.*, vol. 40, no. 4, 223–226, (1978).
- [6] J. Preskill, M. B. Wise, and F. Wilczek, “Cosmology of the invisible axion,” *Phys. Lett. B*, vol. 120, no. 1–3, 127–132, (1983).
- [7] L. F. Abbott and P. Sikivie, “A cosmological bound on the invisible axion,” *Phys. Lett. B*, vol. 120, no. 1–3, 133–136, (1983).
- [8] M. Dine and W. Fischler, “The not-so-harmless axion,” *Phys. Lett. B*, vol. 120, no. 1–3, 137–141, (1983).
- [9] P. W. Graham, I. G. Irastorza, S. K. Lamoreaux, A. Lindner, and K. A. Van Bibber, “Experimental Searches for the Axion and Axion-Like Particles,” *Annu. Rev. Nucl. Part. Sci.*, vol. 65, no. 1, 485–514, (2015).
- [10] D. Kim, J. Jeong, S. W. Youn, Y. Kim, and Y. K. Semertzidis, “Revisiting the detection rate for axion haloscopes,” *J. Cosmol. Astropart. Phys.*, vol. 2020, no. 3, (2020).
- [11] T. Braine *et al.*, “Extended Search for the Invisible Axion with the Axion Dark Matter Experiment,” *Phys. Rev. Lett.*, vol. 124, no. 10, 101303, (2020).
- [12] L. Zhong *et al.*, “Results from phase 1 of the HAYSTAC microwave cavity axion experiment,” *Phys. Rev. D*, vol. 97, no. 9, 92001, (2018).
- [13] D. Alesini *et al.*, “Galactic axions search with a superconducting resonant cavity,” *Phys. Rev. D*, vol. 99, no. 10, 101101, (2019).
- [14] J. Golm *et al.*, “Thin Film (High Temperature) Superconducting Radiofrequency Cavities for the Search of Axion Dark Matter,” 3–7, (2021).
- [15] D. Ahn *et al.*, “Maintaining high Q-factor of

[16] superconducting  $\text{YBa}_2\text{Cu}_3\text{O}_{7-x}$  microwave cavity in a high magnetic field," 1–4, (2019).

[17] R. Di Vora *et al.*, "A high-Q microwave dielectric resonator for axion dark matter haloscopes," 1–8, (2022).

[18] D. Alesini *et al.*, "Realization of a high quality factor resonator with hollow dielectric cylinders for axion searches," *Nucl. Instruments Methods Phys. Res. Sect. A Accel. Spectrometers, Detect. Assoc. Equip.*, vol. 985, no. April 2020, 164641, (2021).

[19] S. Posen and D. L. Hall, "Nb<sub>3</sub>Sn superconducting radiofrequency cavities: fabrication, results, properties, and prospects," *Supercond. Sci. Technol.*, vol. 30, no. 3, 033004, (2017).

[20] D. C. Mattis and J. Bardeen, "Theory of the Anomalous Skin Effect in Normal and Superconducting Metals," *Phys. Rev.*, vol. 111, no. 2, 412–417, (1958).

[21] C. Benvenuti *et al.*, "Magnetic Flux Trapping in Superconducting Niobium," (1997).

[22] M. Martinello *et al.*, "Trapped flux surface resistance for different surface treatments," *Proc. Seventeenth Int. Conf. RF Supercond.*, vol. MOPB015, (2015).

[23] B. Aune *et al.*, "Superconducting TESLA cavities," *Phys. Rev. Spec. Top. - Accel. Beams*, vol. 3, no. 9, 092001, (2000).

[24] R. Brinkmann *et al.*, "TESLA XFEL, First Stage of the X-Ray Laser Laboratory, Technical Design Report," Hamburg, (2001).

[25] J. N. Galayda (ed.), "LCLS-II Final Design Report, LCLSII-1.1-DR-0251-R0." 2015.

[26] "Oxford Instruments," [www.oxinst.com](http://www.oxinst.com) .

[27] C. Bartram *et al.*, "Letter of Interest for Axion Dark Matter eXperiment (ADMX) 2-4 GHz," *Snowmass 2021*, (2021).

[28] A. C. Crawford, "Extreme diffusion limited electropolishing of niobium radiofrequency cavities," *Nucl. Instruments Methods Phys. Res. Sect. A Accel. Spectrometers, Detect. Assoc. Equip.*, vol. 849, no. January, 5–10, (2017).

[29] "ATI Metals," [www.atimetals.com](http://www.atimetals.com) .

[30] P. J. Lee, P. O'Larey, W. Starch, and D. C. Larbalestier, "A flash radiograph standard for Nb-Ti alloys," *Report SMRG 116, The Applied Superconductivity Center The University of Wisconsin-Madison, A Flash Radiograph Standard developed for the SSC*. 1992.

[31] S. Calatroni, "A Mathematica Notebook for the calculation of the anomalous skin effect in copper The Mathematica Notebook Theoretical background," *CERN-ACC-NOTE-2020-0029*, (2020).

[32] A. Godeke, "A review of the properties of Nb<sub>3</sub>Sn and their variation with A15 composition, morphology and strain state," *Supercond. Sci. Technol.*, vol. 19, no. 8, R68–R80, (2006).

[33] A. Romanenko, A. Grassellino, O. Melnychuk, and D. A. Sergatskov, "Dependence of the residual surface resistance of superconducting radio frequency cavities on the cooling dynamics around  $T_c$ ," *J. Appl. Phys.*, vol. 115, no. 18, 184903, (2014).

[34] M. Peiniger, M. Hein, N. Klein, G. Müller, H. Piel, and P. Thuns, "Work on Nb<sub>3</sub>Sn cavities at Wuppertal," in *Proceedings of The Third Workshop on RF Superconductivity*, 1988.

[35] J. Knobloch, "Advanced thermometry studies of superconducting RF cavities," Cornell University, 1997.

[36] H. Padamsee, J. Knobloch, and T. Hays, *RF superconductivity for accelerators*. New York: Wiley-VCH, 2008.

[37] A. Romanenko and D. I. Schuster, "Understanding Quality Factor Degradation in Superconducting Niobium Cavities at Low Microwave Field Amplitudes," *Phys. Rev. Lett.*, vol. 119, no. 26, 1–6, (2017).

[38] A. Alimenti *et al.*, "Surface Impedance Measurements on Nb 3 Sn in High Magnetic Fields," *IEEE Trans. Appl. Supercond.*, vol. 29, no. 5, (2019).

[39] "Comsol," [www.comsol.com](http://www.comsol.com) .